Desalination and Water Treatment
www.deswater.com

doi: 10.5004/dwt.2023.29698

299 (2023) 128–136
July

Adsorption of SO_4^{2-} on Li_2CO_3 crystal surfaces: experiments and first-principles calculation

Xin Liu[a,b,c], Yanfang Ma[b,c,d,*], Yongming Zhang[b,c], Xiuping Ding[b,c], Zhihong Zhang[b,c]

[a]*University of Chinese Academy of Sciences, Beijing 100190, China, email: liuxin192@mails.ucas.ac.cn (X. Liu)*
[b]*Key Laboratory of Comprehensive and Highly Efficient Utilization of Salt Lake Resources, Qinghai Institute of Salt Lakes, Chinese Academy of the Sciences, Xining 810008, China, emails: mayanfag@isl.ac.cn (Y. Ma), yming@isl.ac.cn (Y. Zhang), dingxp@isl.ac.cn (X. Ding), zhangzh@isl.ac.cn (Z. Zhang)*
[c]*Key Laboratory of Salt Lake Resources Chemistry of Qinghai Province, Xining 810008, China*
[d]*Innovation Academy for Green Manufacture, Chinese Academy of Sciences, Beijing 100190, China*

Received 11 December 2022; Accepted 10 June 2023

ABSTRACT

Salt lake brine is an important raw material for Li_2CO_3 preparation, however, the composition of salt lake brine is relatively complicated, and the coexistence of impurity ions affects the quality of Li_2CO_3 crystals. Especially, SO_4^{2-} in brine can compete with CO_3^{2-} to form ion pairs, which limits the nucleation of carbonate. Therefore, it is necessary to study the adsorption behavior of SO_4^{2-} in brine on the surface of Li_2CO_3 crystals. In this paper, the effect of SO_4^{2-} on Li_2CO_3 crystals under different SO_4^{2-}/Li^+ ratios is studied by combining experiments and first-principles calculation. The results show that in the Li_2CO_3 crystallization system, SO_4^{2-} interacts strongly with the crystal surface, which is regarded as chemical adsorption. And because of the SO_4^{2-} is a soluble anion, its elution rate is about 50%. The adsorption of SO_4^{2-} on the surface of Li_2CO_3 affects the morphology, particle size, and purity of the crystals. The governing equation is constructed by the change of the crystal specific surface area with the SO_4^{2-}/Li^+ ratio, which can effectively predict the crystal size and specific surface area with SO_4^{2-} content. The first-principles calculation reveals the microscopic behavior of SO_4^{2-} adsorption on the crystal surface from the molecular level that there is charge transfer between the O atoms of SO_4^{2-} and the Li atoms on the crystal surface, and there is a strong interaction between them.

Keywords: Li_2CO_3; SO_4^{2-}; First-principles calculation; Surface adsorption

1. Introduction

Li_2CO_3 is commonly used as the raw material for the production of inorganic and organic lithium compounds due to its stability and simple form [1,2]. Li_2CO_3 is mainly extracted from lithium ore and salt lake brine as raw materials, and the reserves in liquid form reach 70%, becoming an important raw material for the preparation of Li_2CO_3 [3–5]. Li_2CO_3 products are usually obtained by crystallization of Na_2CO_3 and Li-rich brine. At present, Li_2CO_3 is widely used in industrial fields, especially in some high-tech fields where higher requirements are put forward for the purity, particle size and morphology of Li_2CO_3 products [6–8]. However, impurity ions such as Na^+, Mg^{2+}, Cl^-, K^+ and SO_4^{2-} are contained in salt lake brine, which has a bad influence on the performance of high-purity Li_2CO_3 products, especially in the production and applications of lithium batteries, which greatly affects the electrochemical performance of the batteries [9–12]. Therefore, the impurity effect in the extraction process of Li_2CO_3 has become an important research direction.

* Corresponding author.

The effect of impurity ions was mainly reflected in the selective adsorption of impurity ions on the crystal surface, which changes the growth rate of the crystal surfaces; even the rapidly growing crystal surfaces may disappear as the finally exposed crystal surfaces determine the crystal morphology [13]. During crystallization, due to the presence of impurity ions in the liquid phase, the ions in solution may increase the supersaturation of the solution through salting out or by chemical interactions between ions, and the solubility of the crystal changes [14,15]. In the extraction process used for Li_2CO_3, although only low concentrations of SO_4^{2-} and part of SO_4^{2-} as soluble anions (such as Cl^- and part of SO_4^{2-}) remain after washing with pure water [16], the residual SO_4^{2-} can be concentrated in the subsequent evaporation and concentration process, leading to the precipitation of Li_2SO_4, which affects the yield of Li products and the enrichment degree of Li [17]. Due to the shape of SO_4^{2-}, more than one O atom of SO_4^{2-} could interact with Li atoms on the surface of Li_2CO_3. Moreover, studies had found that SO_4^{2-} can form ion pairs with Li^+ better than with Na^+ in solution, and the formation of such ion pairs largely limits the nucleation of carbonate [18].

Wei et al. [14] and Li et al. [19] reported that SO_4^{2-} is mainly adsorbed on the crystal surface of Li_2CO_3, although 90% SO_4^{2-} in the Li_2CO_3 crystals can be removed by recrystallization and a hydrothermal method. However, studies have shown that the formation of ion pairs among components of sulfate hemihydrate significantly changes the ability of Li_2CO_3 to form from aqueous solution [16,20]. At present, there are few studies on the effect of a low content of SO_4^{2-} on Li_2CO_3 crystals.

This research was based on the Li^+, Na^+//Cl^-, CO_3^{2-}-H_2O crystallization system, and the interaction between SO_4^{2-} and the Li_2CO_3 crystal surface was calculated by first-principles calculation. Through experiments and theoretical calculation, the impurity effect of SO_4^{2-} in the Li_2CO_3 crystallization process under different SO_4^{2-}/Li^+ ratios had been studied. The results can predict the influence rule of SO_4^{2-} on the size and morphology of Li_2CO_3 crystals under different SO_4^{2-}/Li^+ ratios, which is of guiding significance to improve the utilization rate of Li resources and the quality of Li_2CO_3 crystals obtained from salt lake brine.

2. Materials and methods

2.1. Materials

The raw materials used in this study are lithium chloride (LiCl), sodium carbonate (Na_2CO_3), and sodium sulfate (Na_2SO_4). All chemical reagents were analytically pure (≥99.0). Deionized water (resistivity 18.25 mω·cm) was prepared using a water purification system (UPT-II-20T, Chengdu Ultrapure Technology Company Limited.

2.2. Experimental methods

After the deep impurity removal, SO_4^{2-}/Li^+ in Li-rich brine was about 0.5~1, so studied the influence of SO_4^{2-} on Li_2CO_3 within the range of this ratio. The composition of brine is shown in Table 1. Li_2CO_3 crystals were prepared by reaction crystallization of an 18% LiCl solution and a 22% Na_2CO_3 solution in a crystallizer. Under the conditions of a water bath temperature of 80°C, and a specific amount of mother liquor (18% LiCl and 22% Na_2CO_3 saturated NaCl solution after preparation of the mother liquor) was added to the crystallizer for stirring and mixing. The stirring impeller is located in the middle of the mould guide barrel, and the speed is 700 r·min^{-1}. The LiCl solution and different concentrations of sulfate solution (Na_2SO_4 and Na_2CO_3 mixed solutions) are injected at 3.6 and 6 mL·min^{-1} with a peristaltic pump, respectively. After addition, the reaction mixture was stirred for 30 min. The distilled water was heated to 80°C and the obtained solid was washed twice with three times distilled water and then dried. The experimental device is shown in Fig. 1. The SO_4^{2-}/Li^+ ratio conditions in the Li_2CO_3 reactive crystallization system was shown in Table 2. The systems incorporating SO_4^{2-} are labeled as S0 (SO_4^{2-}/Li^+: 0), S1 (SO_4^{2-}/Li^+: 0.05), S2 (SO_4^{2-}/Li^+: 0.5), S3 (SO_4^{2-}/Li^+: 0.8), and S4 (SO_4^{2-}/Li^+: 1), respectively.

The contents of elements in the solid-phase products obtained from reactive crystallization were determined by inductively coupled plasma optical emission spectroscopy (ICP-OES) (Thermo Fisher ICP6500 DUO). The samples were analyzed by X-ray diffraction (XRD) (X'Pert Pro MPD), using Cu-Kα radiation (λ = 1.5406 A). The particle size distribution and morphology of the samples were determined using a Malvern laser particle size analyzer (MS 3000) and a scanning electron microscope (Hitachi SU8010). The chemical composition and atomic content of the solid surface were analyzed by X-ray photoelectron spectroscopy (XPS) (Thermo Scientific K-Alpha). Using a full spectrum scan with a passing energy of 100 eV and a step size of 1 eV. The specific surface area of the solids is analyzed using an automatic specific surface and pore size distribution analyzer (Autosorb-iQ).

2.3. Computational methods

The ideal Li_2CO_3 crystal is monoclinic (space group C2/c). In this study, all the calculations are performed in the framework of DFT with the Projector Augmented Wave method (PAW), as implemented in VASP [21]. The generalized gradient approximation proposed by Perdew, Burke, and Ernzerhof was selected for the exchange-correlation potential (GGA-PBE) [22]. The cut-off energy of the plane wave is set to 400 eV. In the iterative solution of the Kohn-Sham equation, the convergence criterion is set to 10^{-6} eV. The lattice constants of Li_2CO_3 crystals are a = 8.317 Å,

Table 1
Composition of lithium-rich brine system after deep de-impurity

Composition	Content (mol·L^{-1})
Li^+	4.73
Cl^-	4.66
Na^+	4.91
Mg^{2+}	0.18
K^+	0.39
CO_3^{2-}	2.71
SO_4^{2-}	0.061~0.31
H_2O	33.33

b = 4.957 Å, c = 6.046 Å, β = 114.617°, which are consistent with other studies [23]. A 2 × 3 × 2 Li_2CO_3 supercell model was constructed to calculate the surface energy of the crystal. The surface atoms were relaxed and the bottom atoms were fixed. In order to avoid the interaction between adjacent layers, the 15 Å thick vacuum layer was introduced in the *Z*-direction. Brillouin region integration is performed using a 2 × 2 × 1 K-point grid. The valence electrons and their orbitals involved in calculation of the system are: Li: $2s^1$, O: $2s^22p^4$, C: $2s^22p^2$, S: $3s^23p^4$.

The surface energy can provide important information on the stability of the surface structure and is an important physical quantity for studying the material surface, and calculating the surface energy of each surface of the crystal to determine the structure with the lowest surface energy and the most stable crystal plane orientation. The crystal surface energy (J·m^{-2}) under dry conditions is defined by Eq. (1) [24,25].

$$E_{surf} = \frac{E_{slab} - nE_{bulk}}{2A} \quad (1)$$

where E_{slab} refers to the total energy of the surface, E_{bulk} refers to the energy of bulk Li_2CO_3 calculated by optimizing the bulk structure, n refers to the total number of effective atoms in the crystal cell model, and A refers to the optimized area of the crystal face exposed by cutting the crystal.

The adsorption energy of SO_4^{2-} and the Li_2CO_3 crystal surface can represent the relative strength of intermolecular interactions [26]. The adsorption intensity of SO_4^{2-} on the crystal surface has been investigated, and the adsorption energy (eV) is defined as shown in Eq. (2) [27,28].

Table 2
SO_4^{2-}/Li^+ ratios in the Li_2CO_3 reaction crystallization system

Ion content	Sample				
	S0	S1	S2	S3	S4
LiCl (mol·L^{-1})	4.67	4.65	4.64	4.65	4.66
Na_2CO_3 (mol·L^{-1})	2.60	3.45	3.50	3.39	3.46
Li^+ (%)	0.53	0.53	0.53	0.53	0.52
SO_4^{2-} (%)	0	0.03	0.28	0.42	0.55
SO_4^{2-}/Li^+	0	0.05	0.5	0.8	1

$$E_{ads} = E_{surface+absorbate} - \left(E_{surface} + E_{absorbate}\right) \quad (2)$$

where E_{ads} refers to the adsorption energy, $E_{surface + absorbate}$ refers to the total energy absorbed by the adsorbed material on the crystal surface, $E_{surface}$ refers to the surface energy of the crystal, and $E_{absorbate}$ refers to the energy of absorbing material. The more negative the E_{ads} value, the stronger the interaction, indicating that SO_4^{2-} is more easily adsorbed on the Li_2CO_3 surface [29].

3. Results and discussion

3.1. Influence of SO_4^{2-} on Li_2CO_3 crystals

This paper has studied the incorporation of SO_4^{2-} with different SO_4^{2-}/Li^+ ratios in the reactive crystallization process of Li_2CO_3 to explore the influence of SO_4^{2-} ion on Li_2CO_3 crystals. Fig. 2 shows the XRD patterns of Li_2CO_3 crystals obtained at different SO_4^{2-}/Li^+ ratios. The XRD diffraction peaks of the samples were basically consistent with the standard pattern (PDF 98-010-0324) [2], which shows that the structures of the Li_2CO_3 crystals were not changed by the ion effect after adding a certain proportion of sulfate. Due to the low content of SO_4^{2-}, it was not detected by XRD analysis.

The content of SO_4^{2-} in the Li_2CO_3 samples that crystallized under different SO_4^{2-}/Li^+ ratios was analyzed by ICP-OES, and the elution rate of SO_4^{2-} and the purity change of the sample before and after washing were analyzed, and

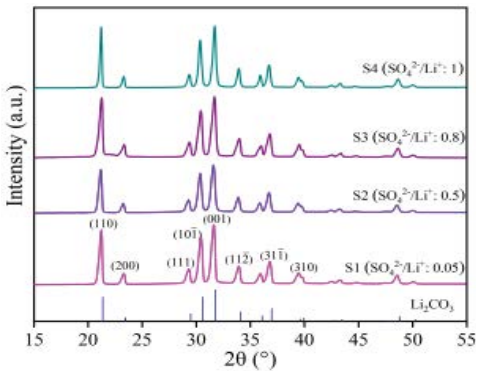

Fig. 2. X-ray diffraction patterns of Li_2CO_3 at different SO_4^{2-}/Li^+ ratios.

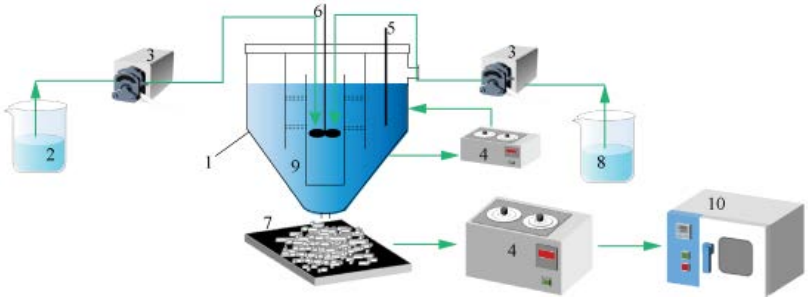

Fig. 1. Diagram of the experimental set-up: (1) crystallizer, (2) mixed solution of Na_2CO_3 and Na_2SO_4, (3) peristaltic pump, (4) thermostatic water bath, (5) thermometer, (6) stirring paddle, (7) Li_2CO_3 crystals, (8) LiCl solution, (9) mother liquor, (10) drying oven.

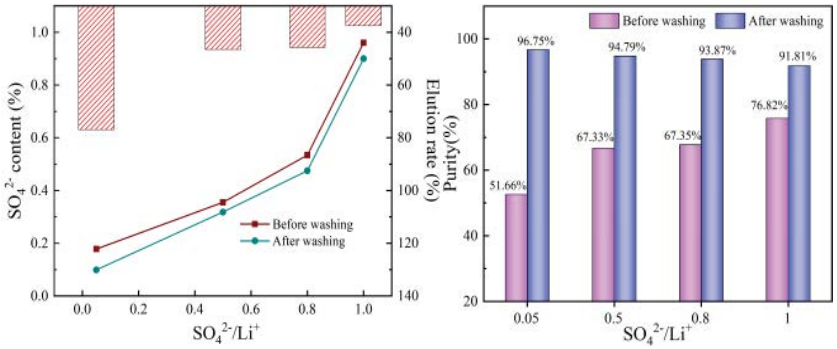

Fig. 3. The SO_4^{2-} content of Li_2CO_3 crystals before and after washing: (a) SO_4^{2-} content and elution rate and (b) purity of Li_2CO_3.

the results are shown in Fig. 3. The results indicate that after washing twice with distilled water, the elution rate of SO_4^{2-} in the crystal is 38.5%~75.5% (Fig. 3a), and the purity of Li_2CO_3 crystals increased by 87.3%~19.5%, due to the elution rate of impurity ions increase (Fig. 3b). The larger the SO_4^{2-}/Li^+ ratio, the lower the elution rate of SO_4^{2-} and leads to the increase in the rate of crystal purity is lower, which indicates that when the content of SO_4^{2-} is high, leads to interact ions between SO_4^{2-} and the crystal surface easily. The SO_4^{2-} in Li_2CO_3 crystals is easy to elute because of SO_4^{2-} is a soluble anion [16], and the solubility of Li_2SO_4 in water increases on increasing the temperature. This is contrary to the solubility of Li_2CO_3, therefore, after washing the solid sample with distilled water at 80°C, about 50% SO_4^{2-} in Li_2CO_3 crystals can be removed.

As shown in Fig. 4, the crystal size of Li_2CO_3 increases on increasing the SO_4^{2-}/Li^+ ratio, and the particle size distribution gradually became wider. The specific surface area of the crystal decreases with an increase of the particle size (as shown in Fig. 5). With an increase in the amount of SO_4^{2-} in the process of Li_2CO_3 reaction crystallization, the change in the specific surface area of Li_2CO_3 crystals also explains why the purity of Li_2CO_3 crystals before washing increases with an increase of the SO_4^{2-}/Li^+ ratio (Fig. 3b). When the SO_4^{2-}/Li^+ ratio was smaller, the purity of the Li_2CO_3 crystals before washing is lower, because the large specific surface area of the crystal, which provides favorable conditions for impurity adsorption. However, the higher impurity elution rate indicates that the impurity ions were mainly coated on the crystal surface in the form of soluble solids, but they did not participate in strong chemical reactions with the ions on the crystal surface. As the SO_4^{2-}/Li^+ ratios increase to 0.8–1, the specific surface areas of the crystal gradually decrease, and the adsorption amount of impurities increases. However, there is a strong interaction between SO_4^{2-} and the crystal surface, which leads to a decrease in the elution rate of the SO_4^{2-}.

In order to explore the adsorption behavior of SO_4^{2-} on the surface of Li_2CO_3 crystals, XPS was used to analyze the surface composition of the Li_2CO_3 samples under different SO_4^{2-}/Li^+ conditions, Fig. 6 shows the XPS spectrum of Li_2CO_3. According to the analysis in Fig. 6a, O 1s was the most significant in the vicinity of 531.34 eV in the four groups of samples, followed by C 1s near 289.28 eV, indicated that the main composition of the crystal surface of Li_2CO_3

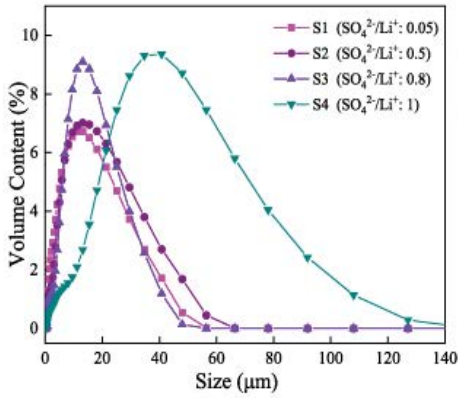

Fig. 4. Li_2CO_3 crystal size distribution curve.

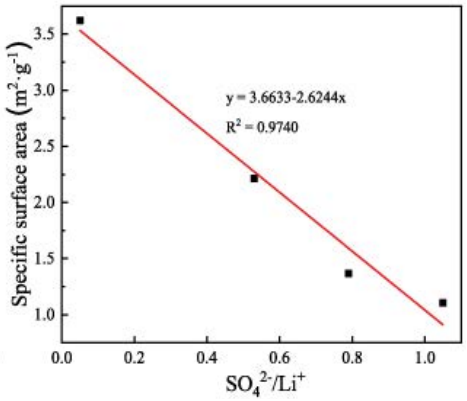

Fig. 5. Specific surface areas of Li_2CO_3 crystals.

doped with SO_4^{2-} was still composed of CO_3^{2-}. As shown in Fig. 6b, with an increase in the SO_4^{2-}/Li^+, the peak value of S 2p increases significantly, which shows that after SO_4^{2-} is incorporated into the crystals, the sulfur on the surface of the crystals has increased to a certain degree.

The data in Table 3 shows the composition and SO_4^{2-} concentration on the surface of Li_2CO_3 crystals by XPS analysis, and the surface concentration of SO_4^{2-} was calculated from Eq. (3) [19].

$$\omega_{SO_4^{2-}} = \frac{x_S \times M\left(SO_4^{2-}\right)}{x_C \times M\left(Li_2CO_3\right) + x_S \times M\left(Li_2SO_4\right)} \times 100\% \quad (3)$$

where $\omega_{SO_4^{2-}}$ represents the molar concentration of SO_4^{2-}, x_S and x_C, respectively represents the atomic fractions of *S* and *C* on the crystal surface, and $M(SO_4^{2-})$, $M(Li_2CO_3)$, $M(Li_2SO_4)$ are the molar masses of SO_4^{2-}, Li_2CO_3, and Li_2SO_4, respectively.

It can be seen from Table 3 that the content of SO_4^{2-} on the crystal surface increases gradually, and the C/S ratio decreases from 89.71 to 29.11, indicating that the higher the SO_4^{2-} content, the stronger is the adsorption strength of SO_4^{2-} on the surface of the Li_2CO_3 crystals.

As shown in Fig. 7, the effect of SO_4^{2-} on the morphology of Li_2CO_3 crystals after washing was investigated. When the SO_4^{2-}/Li^+ ratio was 0.05–0.5 (Fig. 7S1–S2), SO_4^{2-} had minimal effect on the crystal morphology of Li_2CO_3. The crystal is a long prismatic structure, and the crystal surface is smooth. When the SO_4^{2-}/Li^+ ratio was 0.8–1 (Fig. 7S3–S4), the degree of crystal agglomeration increases and there were small particles embedded in the crystal, and many irregular holes appear on the Li_2CO_3 surface, which easily led to impurities into the pores, resulting in the decrease of impurity ion elution rate. The reason for SO_4^{2-} causing crystal surface defects is that SO_4^{2-} is enriched on the crystal surface, which changes the properties of the crystal surface layer and prevents the growth of some lattice surfaces of the crystal, while the irregular holes on the crystal surface make it easier for impurity ions to enter and difficult to remove. Defects on the crystal growth surface often provide nucleation sites for branches. The embedding and agglomeration of crystal particles usually occurs in the competitive process between aggregation and crystal growth [30], and the small particles on the crystal surface grow gradually after secondary nucleation on the large crystal surface.

Table 3
Composition of SO_4^{2-} in Li_2CO_3 on the crystal surface

Sample	Relative content (%)					SO_4^{2-} on surface (%)
	Li	S	C	O	C/S	
S1	29.08	0.31	27.81	42.08	89.71	0.015
S2	30.04	0.47	27.15	41.74	57.77	0.023
S3	27.32	0.56	28.29	43.49	50.52	0.026
S4	27.60	0.96	27.95	42.92	29.11	0.044

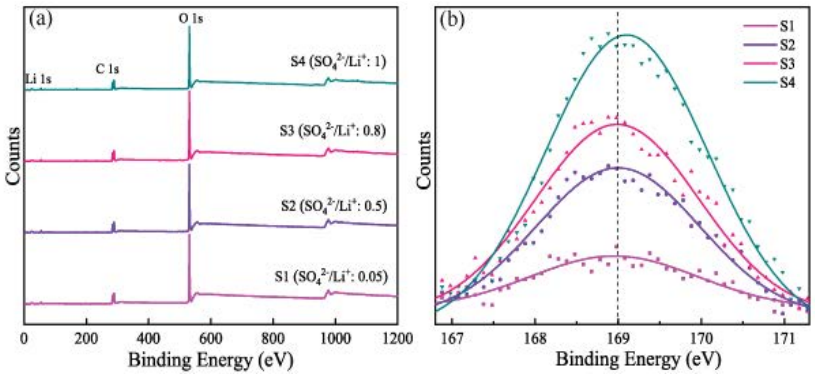

Fig. 6. X-ray photoelectron spectra of Li_2CO_3 crystals: (a) full spectrum and (b) the S 2p spectrum.

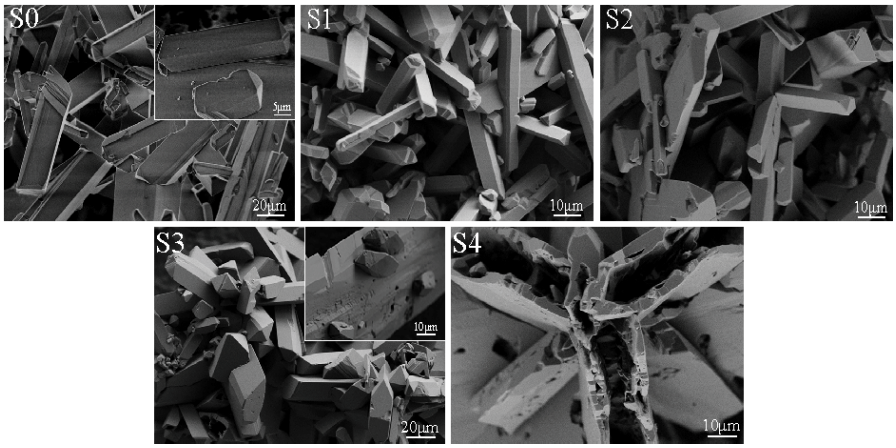

Fig. 7. Scanning electron microscopy images of Li_2CO_3 crystals at different SO_4^{2-}/Li^+ ratios conditions: S0: SO_4^{2-}/Li^+: 0, S1: SO_4^{2-}/Li^+: 0.05, S2: SO_4^{2-}/Li^+: 0.5, S3: SO_4^{2-}/Li^+: 0.8, and S4: SO_4^{2-}/Li^+: 1.

3.2. First-principles calculation study of the adsorption of SO_4^{2-} on the surface of Li_2CO_3

The experimental results shown that SO_4^{2-} is mainly adsorbed on the crystal surface, and the adsorption of impurity ions on the crystal surface has been further studied from the atomic point of view by first-principles calculation. Firstly, the surface energy of each low-index crystal surface in the XRD diagram (as shown in Fig. 2) of the Li_2CO_3 crystals was calculated to analyze the crystal surface stability. Surface energy is a measure of the destruction of chemical bonds that occurs when a surface is formed. The lower the surface energy, the stronger the thermodynamic stability of the surface and the worse the surface activity [31–33]. Fig. 8 shows the surface energy of each crystal surface structure. As shown in Fig. 8, the surface energy of each crystal surface is as follows: (200) > (110) > (111) > $(10\bar{1})$ > (001). In this paper, selected the most stable surfaces (001), $(10\bar{1})$, (111) with the lowest surface energies to study the adsorption of SO_4^{2-} on the surface of Li_2CO_3 crystal.

SO_4^{2-} has two uncoordinated oxygen atoms, and due to its shape, more than one sulfate O atom can interact with Li atoms on the surface of Li_2CO_3 [18]. This study only discusses the adsorption of the Li terminating surfaces (001), $(10\bar{1})$, (111). Fig. 9 shows the stable adsorption configuration of SO_4^{2-} on each surface of the Li_2CO_3 crystals. The most stable adsorption structure was determined by calculating the adsorption energy of each adsorption structure, and the results are shown in Table 4. A negative value for the adsorption energy means that an exothermic reaction has occurred and the adsorption system is stable; a positive value for the adsorption energy means that an endothermic reaction has occurred and the adsorption system is unstable [34,35]. The adsorption energy results shown that when SO_4^{2-} was adsorbed on the (111) surface of the crystals, the adsorption energy was –13.471 eV, and the absolute value of the adsorption energy was higher than that of the (001) and $(10\bar{1})$ surfaces, which indicates that the adsorption configuration is most stable when adsorption occurs on the (111) surface. Therefore, the results shown that the surface atom density of each crystal surface is different, which affects the strength of the interaction between SO_4^{2-} with the Li_2CO_3 surface.

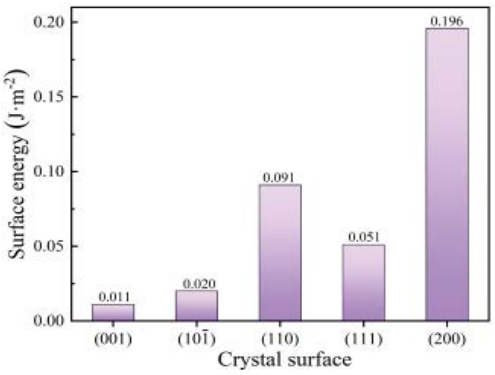

Fig. 8. Surface energy of each surface of the Li_2CO_3 crystals.

The differential charge density can be used to describe the charge distribution, the charge transfer and the bond formation of each atom in the crystal [36,37]. Fig. 10 shows the differential charge density distribution of the SO_4^{2-} stable adsorption model on each surface of Li_2CO_3. In Fig. 10, yellow represents a charge increase and blue represents a charge decrease. It can be seen from Figs. 9 and 10 that during the adsorption process, the O atoms of SO_4^{2-} approach the surface of the Li_2CO_3 crystals and form an ion pair with the Li atoms on the crystal surface. The results shown that more electrons were missing from the Li atom layers of the crystal surface of Li_2CO_3, and the electrons were enriched on the O atoms of SO_4^{2-}. The O atoms of SO_4^{2-} interact with the Li atoms on the crystal surface, and there was charge transfer between the crystal surface and the adsorbed molecule, which indicated that this adsorption mode is chemical adsorption.

Density of state is defined as the number of states that electrons may appear in for a unit energy interval. By analyzing the density of states of a system, we can further understand the mechanism of interaction between SO_4^{2-} and surface atoms [38]. In order to understand the electronic structure changes of SO_4^{2-} on different Li_2CO_3 surfaces, the density of states of SO_4^{2-} adsorbed on different crystal surfaces were calculated, and the results are shown in Fig. 11, where the energy zero point is taken as the Fermi level. It can be seen from Fig. 11a that the density of states of un-adsorbed Li_2CO_3 was symmetric up and down, indicated that Li_2CO_3 is a non-magnetic insulator [18]. Compared with pure Li_2CO_3, a new peak of state density appears in the region close to the Fermi level after SO_4^{2-} was adsorbed on the crystal surface, indicated that the adsorbent had higher

Table 4
Adsorption energies of SO_4^{2-} on each surface of the Li_2CO_3 crystals

Crystal surface	(001)	$(10\bar{1})$	(111)
E_{ads} (eV)	–3.397	–3.693	–13.471

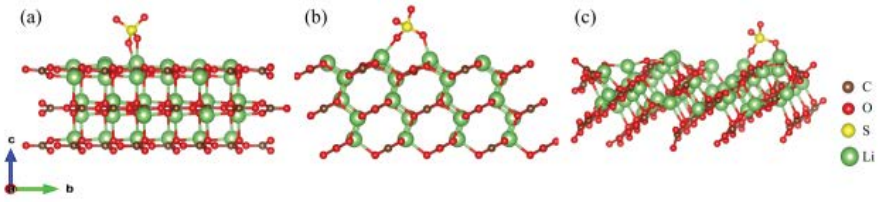

Fig. 9. Stable configurations of SO_4^{2-} adsorbed on each surface of the Li_2CO_3 crystals: (a) the (001) surface, (b) the $(10\bar{1})$ surface, and (c) the (111) surface.

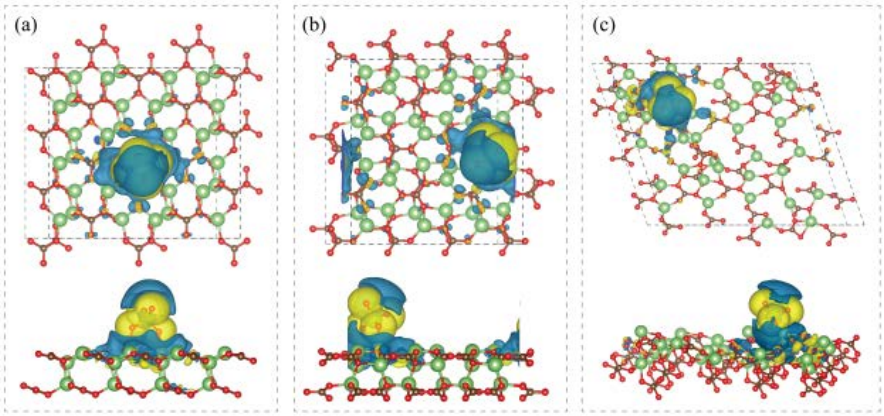

Fig. 10. Charge transfer between SO_4^{2-} and the Li_2CO_3 crystal planes can be illustrated by the differential charge density isosurface (0.0009 e·Å^{-3}) diagram: (a) the (001) surface, (b) the $(10\bar{1})$ surface, and (c) the (111) surface.

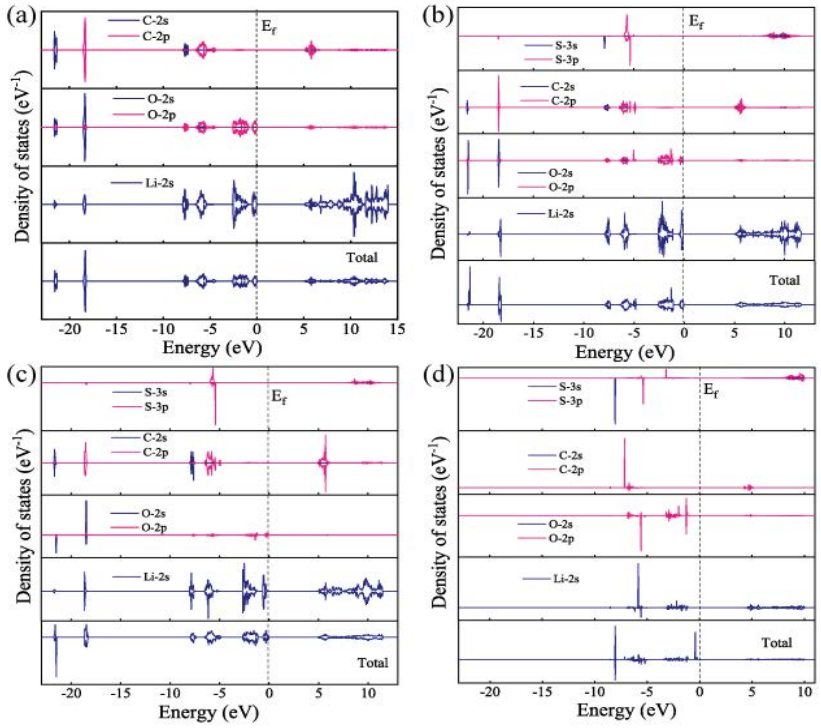

Fig. 11. Density of states of SO_4^{2-} adsorbed on the Li_2CO_3 surface: (a) pure Li_2CO_3 crystals, (b) the (001) surface, (c) the $(10\bar{1})$ surface, and (d) the (111) surface.

reactivity. After SO_4^{2-} was adsorbed on the Li_2CO_3 (001) and $(10\bar{1})$ surfaces (Fig. 11b and c), the contribution of the O-2p and C-2s orbitals decreases significantly, and the density of the Li-2s orbital electron states increases near the Fermi level. After adsorption on the surface (111) (Fig. 11d), the O-2p, C-2p and Li-2s orbitals all had negative displacement, and the peak of electron state density decreases. The negative shifts of the atomic orbitals indicated that the Li atoms of the substrate crystal had a specific effect on SO_4^{2-}. When the SO_4^{2-} was adsorbed on different crystal surfaces, the peak energy level changes and displacements of the orbital energy levels of C, O, and Li atoms indicated that the degree of interaction of SO_4^{2-} on different crystal planes is disparate. The variation and displacement of the density peak of the Li-2s orbital states proved that the presence of SO_4^{2-} has a significant effect on the electron distribution of Li atoms on the crystal surface.

4. Conclusion

The effects of SO_4^{2-} on the morphology, purity, particle size and specific surface area of Li_2CO_3 crystals at different SO_4^{2-}/Li^+ ratios has been studied experimentally and in combination with first-principles calculation to reveal

interactions between atoms in the Li_2CO_3 crystallization system from the molecular level, and to investigate the stable adsorption configuration and adsorption mechanism of SO_4^{2-} on the Li_2CO_3 crystal surface.

- In the Li_2CO_3 reactive crystallization system, SO_4^{2-} can compete with CO_3^{2-} to form Li_2SO_4, resulting in the reduction of crystal purity, and because SO_4^{2-} is a soluble anion, the elution rate is as high as 50%. With the SO_4^{2-}/Li^+ ratio increased, the crystal particle size increased, the specific surface area decreases, and the interaction between SO_4^{2-} and the Li_2CO_3 surface is enhanced. The adsorption of SO_4^{2-} on the surface of Li_2CO_3 crystals inhibits the growth of the crystal lattice surface. When the SO_4^{2-}/Li^+ ratio was 1, there were multiple irregular holes on the crystal surface, which was also an important reason for the decrease of the impurity elution rate in the crystals.
- The adsorption of SO_4^{2-} on the (001), $(10\bar{1})$ and (111) crystal surfaces of Li_2CO_3 has been studied in depth by first-principles calculation. The results shown that there was a strong charge transfer between the Li atom and the O atom of SO_4^{2-} on each crystal surface, and the adsorption structure is relatively stable, which shown that the adsorption form of SO_4^{2-} on the surface of Li_2CO_3 crystals was chemical adsorption. Through analysis of the adsorption energy and density of states diagrams, the adsorption intensity of SO_4^{2-} on the surface of crystal (111) was stronger, indicated that in the actual crystal, SO_4^{2-} adsorbed more easily on the (111) surface, which affects the growth of this lattice surface.

Acknowledgments

This work is supported by the Research and engineering application of "cold crystallization–flotation" process of potassium chloride to improve the adaptability of carnallite ore (grant number KFJ-STS-QYZD-2021-06-002), the Innovation Academy for Green Manufacture, Chinese Academy of Sciences (grant number IAGM2020C01).

References

[1] H. Watamura, H. Marukawa, I. Hirasawa. Polyelectrolyte effects on the crystallization phenomena of the lithium carbonate, J. Crystal Growth, 373 (2013) 111–117.
[2] P. Taborga, I. Brito, T.A. Graber, Effect of additives on size and shape of lithium carbonate crystals, J. Crystal Growth, 460 (2017) 5–12.
[3] P.S. Song, R.J. Xiang, Utilization and exploitation of lithium resources in salt lakes and some suggestions concerning development of Li industries in China, Miner. Deposits, 5 (2014) 977–992.
[4] P.W. Gruber, P.A. Medina, G.A. Keoleian, S.E. Kesler, M.P. Everson, T.J. Wallington, Global lithium availability, J. Ind. Ecol., 15 (2011) 760–775.
[5] H. Vikström, S. Davidsson, M. Höök, Lithium availability and future production outlooks, Appl. Energy, 110 (2013) 252–266.
[6] M. Law, L.E. Greene, J.C. Johnson, R. Saykally, P. Yang, Nanowire dye-sensitized solar cells, Nat. Mater., 4 (2005) 455–459.
[7] Y. Wang, S.C. Du, X.M. Wang, M.M. Sun, Y.J. Yang, J.B. Gong, Spherulitic growth and morphology control of lithium carbonate: the stepwise evolution of core-shell structures, Powder Technol., 335 (2019) 617–628.
[8] M.A. Lovette, A.R. Browning, D.W. Griffin, J.P. Sizemore, R.C. Snyder, M.F. Doherty, Crystal shape engineering, Ind. Eng. Chem. Res., 47 (2008) 9812–9833.
[9] H.Y. Wang, B.Q. Du, M. Wang, Study of the solubility, supersolubility and metastable zone width of Li_2CO_3 in the LiCl–NaCl–KCl–Na_2SO_4 system from 293.15 to 353.15 K, J. Chem. Eng. Data, 63 (2018) 1429–1434.
[10] L.B. Huang, J. Zhu, B.X. Wang, L. Jie, J.C. Liu, T. Yang, Discussion on several processes of preparation of battery grade lithium carbonate from Tibet Salt Lake lithium concentrate, Gansu Metall., 36 (2014) 78–80.
[11] Z.H. Xu, H.J. Zhang, R.Y. Wang, W.J. Gui, G.F. Liu, Y. Yang, Systemic and direct production of battery-grade lithium carbonate from a saline lake, Ind. Eng. Chem. Res., 53 (2014) 16502–16507.
[12] J.W. An, J.K. Dong, K.T. Tran, M.J. Kim, T. Lim, T. Tran, Recovery of lithium from Uyuni salar brine, Hydrometallurgy, 117–118 (2012) 64–70.
[13] S.J. Duan, Multi-Scale Regulation of Reactive Crystallization of Lithium Carbonate, East China University of Science and Technology, 2018.
[14] C. Wei, R.S. Chen, Y.R. Yang, M.G. Yi, L. Xiang, Removal of SO_4^{2-} from Li_2CO_3 by recrystallization in Na_2CO_3 solution, Crystals, 8 (2018) 19, doi: 10.3390/cryst8010019.
[15] C. Wang, Experimental Study on a Series of Lithium Products Obtained from Crude Lithium Sulfate Ore in Salt Pan, University of Chinese Academy of Sciences, 2014.
[16] H.E. King, H. Satoh, K. Tsukamoto, A. Putnis, Nanoscale observations of magnesite growth in chloride- and sulfate-rich solutions, Environ. Sci. Technol., 47 (2013) 8684–8691.
[17] T.L. Ye, Principle and Application of Chemical of Crystallization Process, Beijing University of Technology Press, Beijing, 2006, pp. 78–86.
[18] H.E. King, A. Salisbury, J. Huijsmans, N.Y. Dzade, O. Plümper, Influence of inorganic solution components on lithium carbonate crystal growth, Cryst. Growth Des., 19 (2019) 6994–7006.
[19] X. Li, B. Yuan, M.J. Yi, Study on removal of trace sulfur impurity in lithium carbonate by hydrothermal method, Inorg. Salt Ind., 51 (2019) 4.
[20] G.M. Jiang, H.L. Fu, K. Savino, J.J. Qian, Z.B. Wu, B.H. Guan, Nonlattice cation-SO_4^{2-} ion pairs in calcium sulfate hemihydrate nucleation, Cryst. Growth Des., 13 (2013) 5128–5134.
[21] G. Kresse, D. Joubert, From ultrasoft pseudopotentials to the projector augmented-wave method, Phys. Rev. B: Condens. Matter, 59 (1999) 1758–1775.
[22] J.P. Perdew, K. Burke, M. Ernzerhof, Generalized gradient approximation made simple, Phys. Rev. Lett., 77 (1996) 3865–3868.
[23] Y. Idemoto, J.W. Richardson Jr., N. Kour, S. Kohara, C.-K. Loong, Crystal structure of $(Li_xK_{1-x})_2CO_3$(x = 0, 0.43, 0.5, 0.62, 1) by neutron powder diffraction analysis, J. Phys. Chem. Solids, 59 (1998) 363–376.
[24] Y.H. Chen, C.C. Pan, M.L. Zhang, L.H. Yuan, C.R. Zhang, A first-principles study of the adsorption of H_2 molecules on the surface of $LaFeO_3$, Chin. J. Inorg. Chem., 32 (2016) 945–953.
[25] W.C. Chiou Jr., E.A. Carter, Structure and stability of Fe_3C-cementite surfaces from first principles, Surf. Sci., 530 (2003) 88–100.
[26] Z.Y. Meng, Z.Y. Yang, Z.Q. Yin, Y.Y. Li, X.Q. Ju, Y.Q. Yao, J. Long, Interaction between dispersant and coal slime added in semi-coke water slurry: an experimental and DFT study, Appl. Surf. Sci., 540 (2021) 148327, doi: 10.1016/j.apsusc.2020.148327.
[27] H.W. Gao, S. Pishney, M.J. Janik, First principles study on the adsorption of CO_2 and H_2O on the K_2CO_3 (001) surface, Surf. Sci., 609 (2013) 140–146.
[28] Y.J. Ji, L. Bian, N. Liu, Y.W. Liu, Y.J. Du, Electronic structure of Cs adsorption on $Al_{0.5}Ga_{0.5}N$(0001) surface, Mater. Sci. Semicond. Process., 119 (2020) 105213, doi: 10.1016/j.mssp.2020.105213.

[29] Z.Y. Meng, Z.Y. Yang, X.Q. Ju, X.Y. Song, J. Long, Quantum chemistry study on the influence of dispersants on the pulpability of water coke slurry, J. Fuel Chem. Technol., 47 (2019) 1025–1031.
[30] L. Gránásy, T. Pusztai, G. Tegze, J.A. Warren, J.F. Douglas, Growth and form of spherulites, Phys. Rev. E: Stat. Nonlinear Soft Matter Phys., 72 (2005) 011605, doi: 10.1103/PhysRevE.72.011605.
[31] Y. Shu, Y. Zhang, J.M. Zhang, First-principles analysis of Cu surface properties, J. Phys., 61 (2012) 016108.
[32] Y.M. Zhu, Y.Y. Zhang, N. Nan, R.Q. Xie, J. Liu, First-principles calculations of apatite crystals and surface genes, Metal Mine, 6 (2020) 87–93.
[33] N. Nan, Y.M. Zhu, Y.X. Han, J. Liu, Molecular modeling of interactions between N-(carboxymethyl)-N-tetradecylglycine and fluorapatite, Minerals, 9 (2019) 278, doi: 10.3390/min9050278.
[34] H.W. Wu, N. Zhang, H.M. Wang, S.G. Hong, Adsorption of CO_2 on Cu_2O (111) oxygen-vacancy surface: first-principles study, Chem. Phys. Lett., 568 (2013) 84–89.
[35] W. Zhao, J.D. Wang, F.B. Liu, D.R. Chen, A first-principles study of the adsorption of H_2O molecules on the surface of Fe(100), Fe(110), Fe(111), J. Phys., 58 (2009) 3352–3357.
[36] L. Lin, L.W. Yao, S.F. Li, L.G. Zhu, J.T. Huang, P.T. Wang, W.Y. Yu, C.Z. He, Z. Zhang, The influence of SiC(111) surface with different layers on CH_4 adsorption, Surf. Sci., 702 (2020) 121699, doi: 10.1016/j.susc.2020.121699.
[37] X. Mu, X. Sun, H.M. Li, Z.J. Ding, First-principles study of NO adsorbed Ni(100) surface, J. Nanosci. Nanotechnol., 10 (2010) 7336–7339.
[38] Y.H. Chen, T.T. Liu, M.L.Z. Zhang, B.W. Zhang, C.R. Zhang, M.L. Kang, L. Luo, A first-principles study of the adsorption of H_2 molecules on the surface of Mg_3N_2, J. Chem., 75 (2017) 708–714.